

1 **Venus: A Thick Basal Magma Ocean May Exist Today**

2

3 **J. G. O'Rourke<sup>1</sup>**

4 <sup>1</sup>School of Earth and Space Exploration, Arizona State University, Tempe, AZ, USA.

5 Corresponding author: J. G. O'Rourke ([jgorourk@asu.edu](mailto:jgorourk@asu.edu))

6 **Key Points:**

- 7
- 8 • Extensive melting of the deep mantle during Earth's accretion and differentiation was proposed to solve geochemical and geodynamic puzzles
  - 9 • High temperatures and slow mantle cooling relative to Earth naturally extend the predicted lifetime of a basal magma ocean in Venus
  - 10
  - 11 • A basal magma ocean in Venus would sequester incompatible elements such as potassium and could have sustained a dynamo until recently
  - 12

## 13 **Abstract**

14 Basal magma oceans develop in Earth and Venus after accretion as their mantles solidify from  
15 the middle outwards. Fractional crystallization of the basal mantle is buffered by the core and  
16 radiogenic and latent heat in the magma ocean. Previous studies showed that Earth's basal  
17 magma ocean would have solidified after two or three billion years. Venus has a relatively hot  
18 interior that cools slowly in the absence of plate tectonics, which reduces heat flow through the  
19 solid mantle. Consequentially, the basal magma ocean could remain as thick as ~200–400 km  
20 today. Vigorous convection of liquid silicates could power a global magnetic field until recently  
21 while a core-hosted dynamo is suppressed. The basal mantle ocean may be a hidden reservoir of  
22 potassium and other incompatible elements. A high tidal Love number could reveal a basal  
23 magma ocean and would definitively establish that the core is at least partially liquid.

## 24 **Plain Language Summary**

25 Venus is Earth's nearest neighbor but arguably the least-studied planet in the inner solar system.  
26 Although there are no direct constraints on its deep structure, the mantle of Venus is assumedly  
27 solid by analogy to Earth's current condition. However, recent models of Earth focus on the  
28 prospect that a thick layer of melt called a "basal magma ocean" persisted in the lowermost  
29 mantle for billions of years. This layer cools orders-of-magnitude more slowly than a magma  
30 ocean near the surface because the solid mantle acts as a ~1500-mile-thick blanket. Moreover,  
31 the solid mantle itself remains hot for longer in Venus compared to Earth because its surface is  
32 scorched and desiccated. This study argues that the lifetime of the basal magma ocean in Venus  
33 extends to the present. Detecting a thick, molten layer with future spacecraft missions would  
34 support the hypothesis that Venus and Earth formed under similarly energetic conditions.

## 35 **1 Introduction**

36 Magma oceans were ubiquitous during the formation of rocky planets. Giant impacts,  
37 radiogenic heating, and core formation delivered enough heat to melt entire mantles (e.g., Canup,  
38 2012; Čuk & Stewart, 2012; Elkins-Tanton, 2012; Nakajima & Stevenson, 2015). Crystallization  
39 of the mantle proceeded from the middle outwards because melt is gravitationally stable near  
40 both the surface and core/mantle boundary (CMB) (e.g., Labrosse et al., 2007; Stixrude & Karki,  
41 2005). In particular, bridgmanite crystals are neutrally buoyant at mid-mantle depths where  
42 pressures are ~50 GPa (e.g., Caracas et al., 2019; Mosenfelder et al., 2007). The surficial magma  
43 ocean would have solidified within ~10 or ~100 Myr if it cools directly to space or is blanketed  
44 by a thick steam atmosphere, respectively (e.g., Hamano et al., 2013). In contrast, the basal  
45 magma ocean (BMO) may survive for billions of years because cooling through the solid mantle  
46 is orders-of-magnitude less efficient.

47 Earth's putative BMO has received increasing scrutiny because liquid silicates are a  
48 reservoir of incompatible elements. Labrosse et al. (2007) proposed that a long-lived BMO could  
49 explain differences in  $^{142}\text{Nd}/^{144}\text{Nd}$  ratios between terrestrial rocks and chondritic meteorites and  
50 also solve the so-called "missing heat source" problem (e.g., Korenaga, 2008). Primordial iron-  
51 rich melt (e.g., Zhang et al., 2016) and compositional anomalies (e.g., Li et al., 2017) in the deep  
52 mantle are possibly the last residua of a BMO that has all but finished solidifying.

53 Models that feature a terrestrial BMO predict suppressed cooling of the core and a  
54 delayed start for the geodynamo. While the basal mantle is liquid and thus low viscosity, the  
55 thermal contrast across the CMB is negligible (e.g., Ulvrová et al., 2012). In other words, the

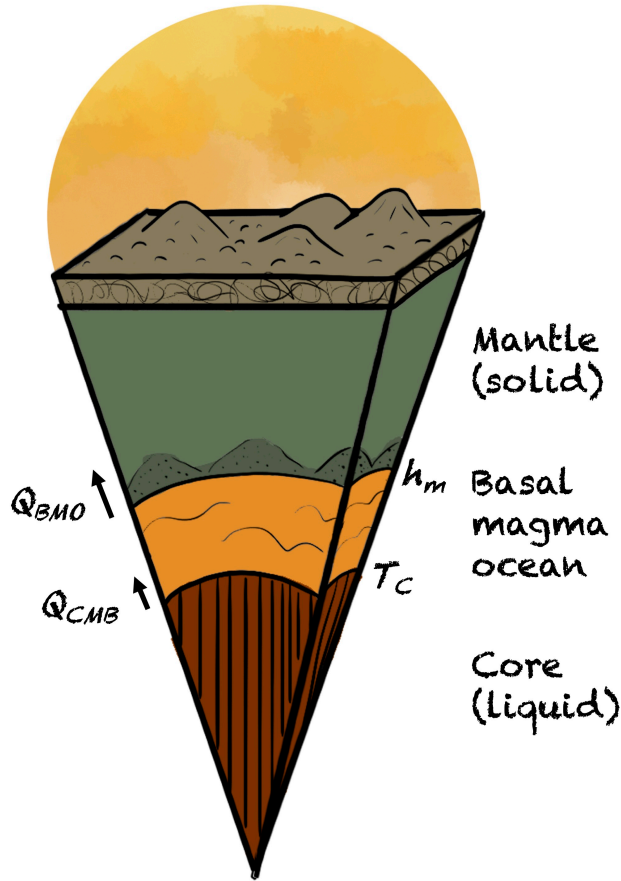
56 BMO and uppermost core should have the same temperature and must cool in tandem. Latent  
57 and radiogenic heat in the BMO buffers its cooling rate, so the core cannot cool rapidly enough  
58 to drive thermal convection until the BMO has started solidifying. Assuming that the BMO was  
59 well-mixed, Labrosse et al. (2007) suggested that convection in Earth's core would not initiate  
60 until ~3.4–4 Gyr ago. Compositional stratification in the BMO could lead to non-continuous  
61 dynamo history with a brief burst of activity before an extended pause (Laneuville et al., 2017).  
62 For now, these predictions stand untested because whether a dynamo existed in the Hadean  
63 and/or Eoarchean is a mystery (e.g., Tang et al., 2019; Weiss et al., 2015).

64 Why would Earth but not Venus have a BMO? These two planets have nearly identical  
65 sizes and bulk densities that are thought to reflect similar bulk compositions (e.g., Smrekar et al.,  
66 2018). Venus likely suffered energetic impacts during accretion although they produced no moon  
67 (e.g., Gillmann et al., 2016; Jacobson et al., 2017). Regardless, gravitational and radiogenic  
68 heating alone were probably sufficient to melt the primordial mantle (e.g., Elkins-Tanton, 2012;  
69 Ikoma et al., 2018). Habitable conditions may have continued until approximately one billion  
70 years ago on Venus (e.g., Way et al., 2016). Alternatively, the proximity of Venus to the Sun  
71 may have delayed solidification of the surficial magma ocean (e.g., Hamano et al., 2013) and  
72 desiccated the atmosphere and surface (e.g., Gillmann et al., 2009). In the absence of colder  
73 temperatures and oceans, Venus entered a geodynamic regime that is less efficient at cooling the  
74 mantle than plate tectonics. Models indicate that the heat flow from the solid mantle to the  
75 surface in Venus is roughly half Earth's modern value, i.e., ~20 TW versus 44 TW (e.g., Driscoll  
76 & Bercovici, 2013, 2014; Gillmann & Tackley, 2014; Weller & Kiefer, 2019). Ultimately, a  
77 BMO should have formed inside Venus and would solidify at a slower rate over time.

78 This study argues that the basal mantle of Venus plausibly remains molten today. Section  
79 2 adapts earlier models of Earth's BMO (Labrosse et al., 2007) and Venus' core (O'Rourke et  
80 al., 2018). The BMO may host a dynamo (e.g., Blanc et al., 2019; Ziegler & Stegman, 2013) if  
81 liquid silicates become semi-metallic at extreme pressures and temperatures (Holmström et al.,  
82 2018; Scipioni et al., 2017; Soubiran & Militzer, 2018). Section 3 presents nominal models for  
83 Earth and Venus. Sensitivity analyses reveal the range of initial thicknesses and temperatures  
84 that are compatible with extant constraints. Section 4 discusses the implications of a BMO for  
85 Venus' geochemistry (e.g., Kaula, 1999), magnetic history (e.g., O'Rourke et al., 2018, 2019),  
86 and tidal response (e.g., Dumoulin et al., 2017). Ultimately, the prospect that a major feature  
87 such as a BMO could await detection highlights the pressing need to explore Earth's near twin.

## 88 **2 Numerical Methods**

89 Figure 1 illustrates the imagined internal structure of Venus. Broadly speaking, the  
90 compositional layering of the deep interior resembles that of Earth roughly two billion years in  
91 the past. No inner core has yet nucleated within Venus—Earth's core only began freezing from  
92 the inside out within the past billion years (e.g., Labrosse, 2015; Nimmo, 2015; O'Rourke et al.,  
93 2017). Fractional crystallization of the BMO enriched the lower mantle in iron. Convection in  
94 the solid mantle of Venus may have organized iron-rich material into thermochemical piles (e.g.,  
95 Labrosse et al., 2007; Li et al., 2017), while the BMO itself remains thick enough to constitute a  
96 global layer with limited topography. However, structural similarities give way to dynamical  
97 differences because modern Venus cools slowly compared to middle-aged Earth. Crucially, the  
98 core and BMO of Venus are entirely stagnant or convecting too sluggishly to drive a dynamo.



99

100 **Figure 1.** Cartoon of the internal structure of Venus. Four key parameters control the thermal  
 101 evolution and any dynamo: the heat flow from the basal magma ocean to the solid mantle  
 102 ( $Q_{BMO}$ ), the heat flow across the core/mantle boundary ( $Q_{CMB}$ ), the temperature at the core/mantle  
 103 boundary ( $T_C$ ), and the height of the basal magma ocean measured from the core/mantle  
 104 boundary ( $h_M$ ). Illustration by JoAnna Wendel.

105

## 106 2.1. Thermal histories

107 Parameterizations of energy sources and sinks are used to track the thermochemical  
 108 evolution of the BMO and core. The Supporting Information describes how the numerical  
 109 methods were adapted from Labrosse et al. (2007) and O'Rourke et al. (2018). To summarize,  
 110 the heat budget of the BMO is

$$111 \quad Q_{BMO} = Q_{SM} + Q_{RM} + Q_{LM} + Q_{CMB}, \quad (1)$$

112 where the heat flow across the solid/liquid interface in the basal mantle ( $Q_{BMO}$ ) is imposed as a  
 113 boundary condition. The first three terms on the right side represent secular cooling ( $Q_{SM}$ ),  
 114 radiogenic heating ( $Q_{RM}$ ), and latent heat ( $Q_{LM}$ ) in the BMO (e.g., Labrosse et al., 2007; Ziegler  
 115 & Stegman, 2013). The heat flow across the CMB ( $Q_{CMB}$ ) comprises additional terms that  
 116 describe the energy budget of the core (e.g., Labrosse, 2015; O'Rourke et al., 2018):

$$117 \quad Q_{CMB} = Q_{SC} + Q_{RC} + Q_{PC} + Q_{GC} + Q_{LC} + Q_{IC}, \quad (2)$$

118 which include secular cooling of the outer core ( $Q_{SC}$ ), radiogenic heating ( $Q_{RC}$ ), and precipitation  
 119 of light species such as magnesium oxide near the CMB ( $Q_{PC}$ ). After nucleation, the inner core  
 120 contributes gravitational energy from the exclusion of light elements ( $Q_{GC}$ ), latent heat ( $Q_{LC}$ ),  
 121 and secular cooling under the assumption of efficient thermal conduction ( $Q_{IC}$ ). Terms  
 122 representing the heat of reaction and pressure changes from thermal contraction are considered  
 123 negligible (e.g., Blanc et al., 2019). Exothermic reactions between the core and BMO such as  
 124 oxygen partitioning (e.g., Pozzo et al., 2019) are also ignored, but could also slow the  
 125 solidification of the BMO. Large amounts of heat could be transported laterally within the BMO  
 126 and core and/or conducted upwards. However, the energy budgets only include heat that crosses  
 127 the CMB or the upper boundary of the BMO because heats that are generated and lost within a  
 128 single layer sum to zero. Labrosse et al. (2007) assumed that  $Q_{CMB}$  was proportional to one  
 129 specific heat for the core, which was held constant. In reality, the effective specific heat of the  
 130 core should decrease over time with radiogenic heating but increase once the inner core  
 131 nucleates. This study avoids that simplification in order to delineate the inner core and dynamo.

132 The key to generating thermal histories is realizing that nearly all of the heat sources are  
 133 directly proportional to the cooling rate of the core. Radiogenic heating is the exception but easy  
 134 to calculate as an absolute value given the initial abundances of heat-producing elements. For all  
 135 other terms in Eq. 1,

$$136 \quad Q_i = \tilde{Q}_i \left( \frac{dT_C}{dt} \right), \quad (3)$$

137 where  $\tilde{Q}_i$  depends only on the thermodynamic properties of the BMO and core (i.e., physical  
 138 constants from Tables S1 and S2) and  $T_C$  is the temperature at the CMB. Secular cooling in the  
 139 BMO is parameterized using a specific heat that is invariant with depth. Latent heat is computed  
 140 with an idealized phase diagram for a well-mixed BMO (Labrosse et al., 2007). Energetic terms  
 141 for the core are derived by integrating fourth-order polynomials, which describe the radial  
 142 density and temperature profiles in the core, over the volume(s) of the outer and/or inner cores  
 143 (e.g., Labrosse, 2015; Nimmo, 2015; O'Rourke et al., 2018). Combining Eq. 1 and 2,

$$144 \quad \frac{dT_C}{dt} = \frac{Q_{BMO} - Q_{RM} - Q_{RC}}{\tilde{Q}_{SM} + \tilde{Q}_{LM} + \tilde{Q}_{SC} + \tilde{Q}_{PC} + \tilde{Q}_{GC} + \tilde{Q}_{LC} + \tilde{Q}_{IC}}. \quad (4)$$

145 This equation places the boundary and initial conditions in the numerator and the structural  
 146 parameters in the denominator. As discussed in the Supporting Information, the thickness of the  
 147 BMO and the radius of the inner core are also directly proportional to  $dT_C/dt$ . Given initial values  
 148 for the size of the BMO and  $T_C$ , the forward Euler method generates a thermal history consisting  
 149 of all the time-dependent quantities listed in Table S3. Timesteps of  $\sim 1$  Myr suffice because  
 150 halving the timestep yielded no discernable change in the model results.

## 151 2.2. Prospects for dynamo action

152 Thermal histories reveal when and where a dynamo could exist. The basic criterion for a  
 153 dynamo is that a rapidly rotating, electrically conductive fluid convects with sufficient vigor.  
 154 Although the rotation of Venus is “slow” relative to Earth, it is “rapid” in the context of dynamo  
 155 physics because the Coriolis force would strongly affect fluid flow in its core and/or BMO as  
 156 expressed by small Rossby numbers ( $\sim 10^{-5} \ll 1$ ) at the equator (e.g., Stevenson, 2003). Simply  
 157 put, the rotation rate of Venus is not to blame for the lack of a strong magnetic field. The  
 158 dynamo criterion thus reduces to convection in the BMO and/or core. If the heat flow across the

159 upper boundary does not exceed that conducted upwards along an adiabatic gradient, then  
 160 thermal conduction—the bane of dynamos—transports heat without fluid motion. Chemical  
 161 sources of buoyancy such as radiogenic heating, precipitation of light elements, and growth of an  
 162 inner core decrease the minimum heat flow required to support a dynamo.

163 There are two general methods for estimating the power of a dynamo. First, scaling laws  
 164 relate the flux of compositional and/or thermal buoyancy to the velocities of convective flows  
 165 (e.g., Christensen, 2010). Higher velocities translate to stronger magnetic fields. Second, entropy  
 166 budgets reveal whether non-zero amounts of dissipation are available for the dynamo (e.g.,  
 167 Labrosse, 2015). Classical thermodynamics explicitly compares the entropy sink associated with  
 168 thermal conductivity to the entropy production from the myriad heat sources. To enable  
 169 straightforward comparisons to previous studies, velocity scalings are applied to the BMO (e.g.,  
 170 Labrosse et al., 2007; Ziegler & Stegman, 2013) while the entropy budget is calculated for the  
 171 core (e.g., O’Rourke et al., 2018). In contrast, Driscoll & Bercovici (2014) used velocity scalings  
 172 for the core while Blanc et al. (2019) recently formulated the entropy budget for the BMO. Either  
 173 method yields similar results. Ultimately, no dynamo exists when the heat flow is sub-critical.

174 Velocity scalings quantify convective vigor within the BMO. The magnetic Reynolds  
 175 number is  $Rm = \mu_0 v_M h_M \sigma_M$ . A dynamo may exist if  $Rm > O(10)$ , where an exact cutoff of 40 is  
 176 commonly used (e.g., Stevenson, 2003). Here  $\mu_0$  is the permittivity of free space and  $h_M$  is the  
 177 thickness of the BMO (e.g., Ziegler & Stegman, 2013). The electrical conductivity ( $\sigma_M$ ) is  
 178 assumed to equal  $2 \times 10^4$  S/M (Holmström et al., 2018; Scipioni et al., 2017; Soubiran &  
 179 Militzer, 2018). Nominal values for the convective velocity ( $v_M$ ) are taken from the scaling based  
 180 on the Coriolis-Inertial-Archimedean (CIA) force balance:

$$181 \quad v_{CIA} = \left( \frac{Q_{BMO}}{\rho_M H_T} \right)^{\frac{2}{5}} \left( \frac{h_M}{\Omega} \right)^{\frac{1}{5}}, \quad (5)$$

182 where  $\rho_M$  is the density of the BMO,  $H_T$  is its thermal scale height, and  $\Omega$  is the planetary  
 183 rotation rate. Scalings based on mixing length theory and the Magnetic-Archimedean-Coriolis  
 184 (MAC) force balance are also considered (Supporting Information). If the  $Rm$ -criterion is  
 185 satisfied, then the magnetic field at the equatorial surface is calculated as

$$186 \quad B_S = \frac{1}{7} (2\varepsilon f_{ohm} \mu_0 \rho_M v_{CIA}^2)^{\frac{1}{2}} \left( \frac{r_B}{r_P} \right)^3, \quad (6)$$

187 where  $\varepsilon$  is a constant prefactor,  $f_{ohm}$  is the fraction of available power that is converted to ohmic  
 188 dissipation as magnetic energy,  $r_B$  is the radial distance from the planetary center to the upper  
 189 boundary of the BMO, and  $r_P$  is the planetary radius (Christensen, 2010). These scalings predict  
 190 Earth-like surface strengths of  $\sim 30$   $\mu$ T for flow velocities of  $\sim 1$  cm/s in the BMO.

191 Entropy budgets determine whether the core is convective. The total dissipation available  
 192 for a dynamo is the sum of various sources and sinks:

$$193 \quad \Phi = \frac{T_{DC} [T_L(r_I) - T_C]}{T_L(r_I) T_C} (Q_{LC} + Q_{IC}) + \frac{T_{DC}}{T_C} (Q_{GC}) + \frac{T_{DC} - T_C}{T_C} (Q_{RC}) + \\ \frac{T_{DC} (T_{SC} - T_C)}{T_{SC} T_C} (Q_{SC}) + \frac{T_{DC}}{T_C} (Q_{PC}) - T_{DC} E_K. \quad (7)$$

194 Here  $T_{DC}$  is the average temperature in the outer core,  $T_L(r_i)$  is the liquidus temperature of the  
 195 core at the inner core boundary, and  $T_{SC}$  is an effective temperature association with dissipation  
 196 from secular cooling. The entropy sink ( $E_K$ ) is associated with and directly proportional to  
 197 thermal conductivity. The thermal conductivity of the core near the CMB is uncertain within a  
 198 broad range:  $\sim 33\text{--}226$  W/m/K (e.g., Konôpková et al., 2016; Ohta et al., 2016). In contrast, the  
 199 thermal conductivity of perovskite at similar conditions is unambiguously lower at  $\sim 10\text{--}20$   
 200 W/m/K (e.g., Ohta et al., 2012). Gravitational energies associated with chemical buoyancy ( $Q_{GC}$   
 201 and  $Q_{PC}$ ) are efficient sources of dissipation that are not penalized by “Carnot-like” efficiency  
 202 terms (e.g., Labrosse, 2015; O’Rourke et al., 2018). The total dissipation is translated into a true  
 203 dipole moment (TDM) using a scaling law that considers the relative amounts of dissipation  
 204 generated at the CMB and inner core boundaries (Aubert et al., 2009). This scaling is only  
 205 approximate because how the dynamo changes once the inner core nucleates remains uncertain  
 206 (e.g., Landeau et al., 2017). In any case, the surface magnetic field at the equator follows as

$$207 \quad B_S = \frac{\mu_0}{4\pi} \left( \frac{\text{TDM}}{r_p^3} \right). \quad (8)$$

208 These formulations assume that flows in the core and BMO are independent. Future studies  
 209 should investigate possible magnetohydrodynamic couplings between flows in both regions.

### 210 **3 Results**

#### 211 **3.1. Models for Earth**

212 Earth is a benchmark for models of Venus. Augmenting Labrosse et al. (2007) with a  
 213 detailed description of the core was the first step in this study. The nominal model was initialized  
 214 with the thickness and temperature of the BMO equaling 750 km and 5250 K, respectively. The  
 215 BMO started with 20 TW of radiogenic heating, which is  $\sim 14\%$  of the total heating expected for  
 216 bulk silicate Earth (e.g., Lay et al., 2008). The core contained 50 ppm of potassium (e.g., Hirose  
 217 et al., 2013) and precipitated light elements at a rate of  $\sim 10^{19}$  kg/K or  $5 \times 10^{-6}$  K $^{-1}$  normalized to  
 218 the mass of the core (e.g., Badro et al., 2018; O’Rourke & Stevenson, 2016). Finally,  $Q_{BMO}$   
 219 decreased linearly from 55 TW at the start to 15 TW at present, which approximates the cooling  
 220 history obtained using boundary layer models (e.g., Blanc et al., 2019; Labrosse et al., 2007;  
 221 Ziegler & Stegman, 2013) and dynamical simulations (e.g., Nakagawa & Tackley, 2010, 2015).

222 Figure S1 shows that this model reproduces major features of Earth’s history. First, the  
 223 globally averaged thickness of the BMO is only  $\sim 1$  km at present (Figure S1c), which is small  
 224 enough that solid-state mantle convection would concentrate the BMO into pockets of primordial  
 225 melt consistent with seismology (Labrosse et al., 2007). Second, the predicted radius of the inner  
 226 core today is 1206 km, close to the correct value of 1220 km (Figure S1d). Third, the inner core  
 227 nucleated  $\sim 500$  Myr ago (Figure S1e) but a dynamo persisted at all times (Figure S1f). If the  
 228 thermal conductivity of the core is relatively low at  $\sim 40$  W/m/K, then a core dynamo always  
 229 operated. Higher thermal conductivity could suppress a core dynamo at early times, but the BMO  
 230 would still host a dynamo with roughly the same strength for the first  $\sim 0.5\text{--}1.5$  Gyr (Figure S1f).

231 Figure S2 reports a sensitivity test for the terrestrial models. Initial values of  $h_M$  and  $Q_{BMO}$   
 232 were varied from  $\sim 600$  to 1500 km and  $\sim 35$  to 60 TW, respectively. Decreasing the heat flow to  
 233 the solid mantle is equivalent to decreasing the amount of radiogenic heating and/or the latent  
 234 heat of solidification in the BMO, so those other parameters were not separately permuted. Key  
 235 outputs were the present-day thickness of the BMO (Figure S2a) and the lifetime of the dynamo

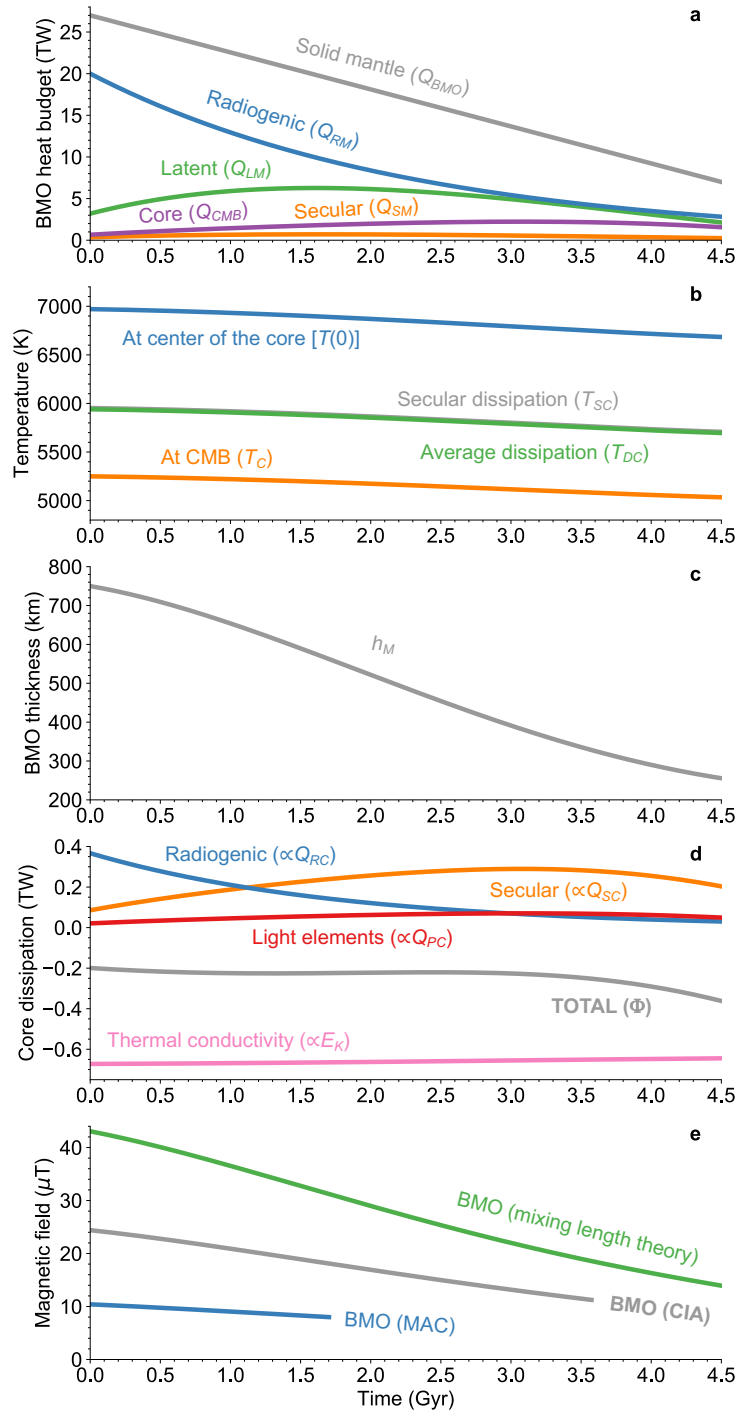
236 in the BMO (Figure S2b). Neither key output was very sensitive to the initial temperature of the  
 237 BMO. Likewise, the thermal history of the BMO does not depend on the particulars of the  
 238 evolution of the core. For example, changing the amount of radiogenic heating or the rate of  
 239 elemental precipitation only adjusts the proportions in which the available heat flow ( $Q_{CMB}$ ) is  
 240 distributed between the various sources. Models are invalidated if  $h_M \geq 10$  km today because  
 241 seismology has revealed no global melt layer in the basal mantle. Ultimately, Earth's BMO could  
 242 have started as thick as  $\sim 1000$  km, in which case a dynamo in the BMO may have survived for  
 243  $\sim 2$  Gyr. Assuming that Earth and Venus accreted in an equivalently energetic environment,  
 244 expecting that the BMO in Venus began with a similar size seems logical.

### 245 3.2. Models for Venus

246 A nominal model for Venus was obtained through two modifications to the terrestrial  
 247 benchmark. First, various structural parameters were adjusted to slightly lower internal pressures  
 248 (Table S2), e.g.,  $\sim 125$  versus 130 GPa at the CMB for Venus and Earth, respectively. Second,  
 249 the heat flow to the solid mantle was halved at all times, i.e.,  $Q_{BMO}$  decreased linearly from 27 to  
 250 7 TW over 4.5 Gyr to match the cooling history in dynamical simulations (e.g., Gillmann &  
 251 Tackley, 2014; O'Rourke et al., 2018). All other model parameters—the initial temperature and  
 252 thickness of the BMO and the potassium content of the core—were held constant. These  
 253 treatments are faithful to the hypothesis that Venus and Earth began as twin planets and then  
 254 diverged because their surficial magma oceans solidified on different timescales.

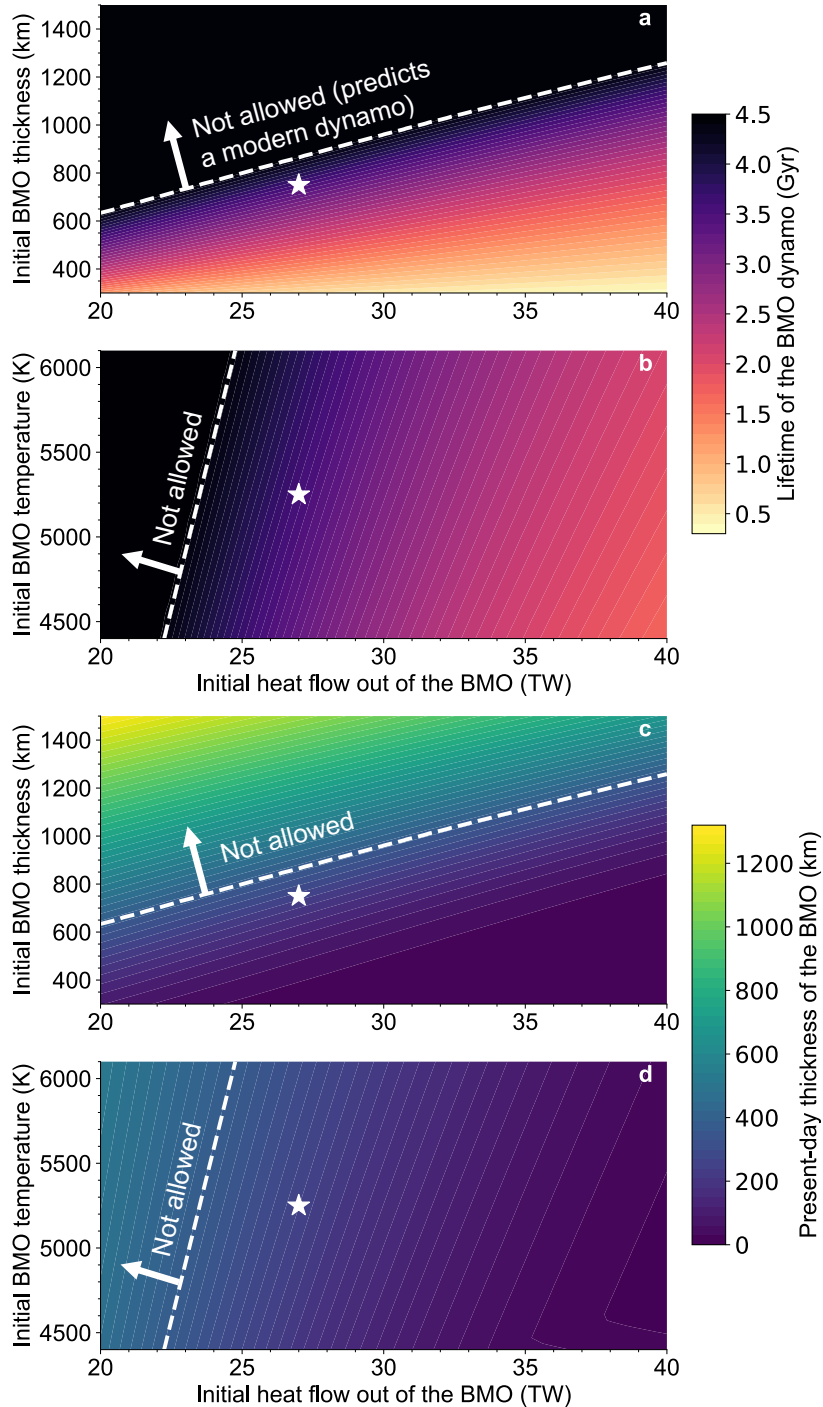
255 Figure 2 elucidates the dramatic consequences of slow mantle cooling for the structure  
 256 and dynamics of the deeper interior. Radiogenic and latent heat dominate the energy budget of  
 257 the BMO (Fig. 2a), so the core and BMO only cool by  $\sim 216$  K over 4.5 Gyr (Fig. 2b). The  
 258 thickness of the BMO decreases by  $\sim 494$  km to  $\sim 256$  km (Fig. 2c), which is deep enough to  
 259 constitute a global layer today. Driving a dynamo in the core with thermal convection alone  
 260 would require  $Q_{CMB} > 4.8$  TW compared to its maximum and modern values of  $\sim 2.2$  and 1.6 TW,  
 261 respectively. Dissipation in the core remains negative at all times (Fig. 2d) even though the  
 262 thermal conductivity was set to the lowest plausible value (40 W/m/K). If there were no BMO,  
 263 then  $Q_{CMB} \sim Q_{BMO}$  and the core would have powered a dynamo at all times. The BMO may have  
 264 hosted a dynamo until recently, although the predicted lifetime depends on the choice of velocity  
 265 scaling law (Fig. 2e). Mixing length theory suggests that a strong dynamo exists today, which is  
 266 incorrect (Phillips & Russell, 1987). In contrast, the MAC scaling indicates that the dynamo died  
 267  $\sim 2.8$  Gyr ago. The favored, CIA scaling suggests that Venus had a magnetic field with surface  
 268 strengths of  $\sim 10$ – $30$   $\mu$ T until  $\sim 0.9$  Gyr ago, less than the estimated ages of many surface units.

269 Figure 3 shares a sensitivity test for these models of Venus. Initial values of  $h_M$  and  $Q_{BMO}$   
 270 were varied again (Fig. 3a and 3c), alongside a range of starting values for  $T_C$  (Fig. 3b and 3d).  
 271 Models were invalidated if the CIA scaling predicted that the BMO would host a dynamo today  
 272 because  $R_m > 40$ . The derived upper limits on the initial thickness of the BMO are similar for  
 273 both Earth and Venus although the criterion for Earth was based on a different requirement:  
 274 complete solidification of the BMO. For Venus, setting  $h_M \leq 860$  km initially would yield  
 275 acceptable models using the nominal cooling history, which return  $h_M \leq 370$  km at present day.  
 276 The upper limit for  $h_M$  increases to  $\sim 1250$  km but decreases to  $\sim 630$  km if  $Q_{BMO}$  is raised or  
 277 lowered initially to 40 or 20 TW, respectively. As for Earth, these results are mostly insensitive  
 278 to the absolute temperature of the BMO. Changing  $T_C$  by  $\sim 1500$  K is equivalent to adjusting  
 279  $Q_{BMO}$  by  $\sim 3$  TW only, so the a priori uncertainty on  $T_C$  is relatively unimportant albeit very large.



280

281 **Figure 2.** Nominal model for Venus. A long-lived basal magma ocean is the natural outcome of  
 282 the conventional cooling history for the solid mantle, which is compatible with the observed lack  
 283 of a strong magnetic field today. (a) Heat budget of the basal magma ocean. (b) Temperatures at  
 284 the core/mantle boundary and deeper in the core. (c) Thickness of the basal magma ocean. (d)  
 285 Dissipation budget for the core including all non-zero terms from Equation 7, which is always  
 286 negative in total. (e) Estimated strength of the magnetic field at the surface based on three  
 287 velocity scalings for the basal magma ocean. The CIA scaling reproduces the lack of a dynamo  
 288 today but further motivates a search for crustal remanent magnetization.



289

290 **Figure 3.** Sensitivity analysis for models of Venus. The maximum thickness of the basal magma  
 291 ocean at present day is  $\sim 400$  km. Models with larger melt layers conflict with observational  
 292 evidence against a strong intrinsic magnetic field. Arrows point towards invalid initial conditions  
 293 on one side of the dashed white lines. Lifetimes of the dynamo in the basal magma ocean are  
 294 estimated with the Coriolis-Inertial-Archimedean velocity scaling as functions of the initial heat  
 295 flow to the solid mantle and the initial (a) temperature and (b) thickness of the basal magma  
 296 ocean. Present-day thicknesses of the basal magma ocean are reported versus its initial (c)  
 297 temperature and (d) thickness. White stars represent the nominal model.

## 298 4 Discussion

299 Future investigations should build on the simplifications that this study employed. In  
300 particular, solidification timescales were estimated with an idealized phase diagram (e.g.,  
301 Labrosse et al., 2007) but actually depend on whether compositional layering develops (e.g.,  
302 Laneuville et al., 2017) and on the partition coefficient for FeO between the BMO and the solid  
303 mantle (e.g., Blanc et al., 2019). Fully dynamical simulations are required to generate self-  
304 consistent cooling histories and track the fate of iron-rich residua in the solid mantle. Despite  
305 these limitations, the likelihood that a BMO persisted within Venus has myriad implications. For  
306 example, incompatible elements from the lowermost ~650–1250 km of the mantle (e.g., ~11–  
307 25% of the mantle’s total volume), including potassium and associated decay products such as  
308 argon-40 (e.g., Kaula, 1999; Namiki & Solomon, 1998; O’Rourke & Korenaga, 2015; Xie &  
309 Tackley, 2004), could remain hidden in a reservoir that surface volcanism and degassing would  
310 not sample. Beyond geochemistry, two other issues deserve particular attention.

### 311 4.1. Tidal response of a basal magma ocean

312 Tidal deformation of Venus constrains the structure of the deep interior. Assuming an  
313 elastic response from the mantle to solar tides, Yoder (1995) predicted that a Love number  $k_2$   
314 above 0.23 would signal that the core is at least partially liquid today. Doppler tracking of the  
315 NASA Magellan and Pioneer Venus Orbiter missions then determined that  $k_2 = 0.295 \pm 0.066$   
316 (Konopliv & Yoder, 1996). However, Dumoulin et al. (2017) recently showed that realistic  
317 viscoelasticity of the mantle strongly increases  $k_2$  relative to predictions from elastic models, so  
318 envisioned missions would need to constrain  $k_2 > 0.27$  to verify that the core is liquid. A BMO  
319 would decouple the solid mantle from the core and, in principle, raise  $k_2$  even if the underlying  
320 core were completely solid. In reality, the solidus of the core is far lower than that of the basal  
321 mantle—no realistic thermal history features a BMO and a solid core (O’Rourke et al., 2018).  
322 Overall, measuring a high  $k_2$  would thus prove that the core remains partially liquid.

### 323 4.2. Magnetic history of Venus

324 Venus could have sustained an Earth-strength magnetic field until recently. O’Rourke et  
325 al. (2018) assumed that the mantle had fully solidified and found that the core would power a  
326 dynamo for billions of years. High thermal conductivity for the core (e.g.,  $>100$  W/m/K) was  
327 invoked because simulations using lower conductivity over-predicted the lifetime of the dynamo.  
328 In this study, a dynamo exists instead in the BMO but survives for similar timescales. Thermal  
329 conductivity of the core is no longer a critical uncertainty because the cooling rate of the core is  
330 sub-adiabatic regardless. Crustal remanent magnetism is a potentially observable consequence of  
331 an early dynamo in either the core or BMO (O’Rourke et al., 2019). Any detection of crustal  
332 magnetization would indicate that Venus and Earth accreted under similarly energetic conditions.  
333 Alternatively, Venus could have accreted under less energetic conditions where any BMO was  
334 short-lived and chemical stratification precluded convection in the core (Jacobson et al., 2017).

## 335 5 Conclusions

336 Earth’s early evolution featured a basal magma ocean that took several billion years to solidify.  
337 Until now these models have not been extended to Venus. Slow mantle cooling in the absence of  
338 plate tectonics on Venus is a common feature of dynamical simulations. The natural consequence  
339 is an extended lifetime for the basal magma ocean. Roughly speaking, halving the cooling rate

340 doubles the solidification timescale. Models indicate that the lowermost ~200–400 km of the  
 341 mantle of Venus plausibly remains molten today. Seismology would enable the direct detection  
 342 of a thick melt layer, which should also yield a high tidal Love number that is degenerate with a  
 343 partially liquid core. The basal magma ocean is a hidden reservoir of incompatible elements that  
 344 the solid mantle will not ingest for billions of years. Vigorous fluid motions in the basal magma  
 345 ocean can drive a dynamo until recent times (<1 Gyr ago), but latent and radiogenic heat keeps  
 346 the cooling rate of the core below the adiabatic limit for a dynamo driven by thermal convection.  
 347 The basal magma ocean gives, and the basal magma ocean has taken away.

### 348 **Acknowledgments**

349 J. G. O'Rourke was supported by the SESE Exploration Postdoctoral Fellowship. Data are  
 350 presented in the main text and supporting information. Jupyter notebooks that run the models for  
 351 Earth and Venus to generate all figures are archived with Zenodo. [Note for review: The code is  
 352 not public now but will be posted upon acceptance of this manuscript.]

### 353 **References**

- 354 Aubert, J., Labrosse, S., & Poitou, C. (2009). Modelling the palaeo-evolution of the geodynamo.  
 355 *Geophysical Journal International*, 179(3), 1414–1428. [https://doi.org/10.1111/j.1365-](https://doi.org/10.1111/j.1365-246X.2009.04361.x)  
 356 [246X.2009.04361.x](https://doi.org/10.1111/j.1365-246X.2009.04361.x)
- 357 Badro, J., Aubert, J., Hirose, K., Nomura, R., Blanchard, I., Borensztajn, S., & Siebert, J. (2018).  
 358 Magnesium Partitioning Between Earth's Mantle and Core and its Potential to Drive an  
 359 Early Exsolution Geodynamo. *Geophysical Research Letters*, 45(24), 13,240–13,248.  
 360 <https://doi.org/10.1029/2018GL080405>
- 361 Blanc, N. A., Stegman, D. R., & Ziegler, L. B. (2019). Thermal and Magnetic Evolution of a  
 362 Crystallizing Basal Magma Ocean in Earth's Mantle. <https://doi.org/10.31223/osf.io/cmgef>
- 363 Canup, R. M. (2012). Forming a Moon with an Earth-like composition via a giant impact.  
 364 *Science*, 338(6110), 1052–5. <https://doi.org/10.1126/science.1226073>
- 365 Caracas, R., Hirose, K., Nomura, R., & Ballmer, M. D. (2019). Melt–crystal density crossover in  
 366 a deep magma ocean. *Earth and Planetary Science Letters*, 516, 202–211.  
 367 <https://doi.org/10.1016/j.epsl.2019.03.031>
- 368 Christensen, U. R. (2010). Dynamo Scaling Laws and Applications to the Planets. *Space Science*  
 369 *Reviews*, 152(1–4), 565–590. <https://doi.org/10.1007/s11214-009-9553-2>
- 370 Čuk, M., & Stewart, S. T. (2012). Making the Moon from a fast-spinning Earth: a giant impact  
 371 followed by resonant despinning. *Science*, 338(6110), 1047–52.  
 372 <https://doi.org/10.1126/science.1225542>
- 373 Driscoll, P., & Bercovici, D. (2013). Divergent evolution of Earth and Venus: Influence of  
 374 degassing, tectonics, and magnetic fields. *Icarus*, 226(2), 1447–1464.  
 375 <https://doi.org/10.1016/j.icarus.2013.07.025>

- 376 Driscoll, P., & Bercovici, D. (2014). On the thermal and magnetic histories of Earth and Venus:  
377 Influences of melting, radioactivity, and conductivity. *Physics of the Earth and Planetary*  
378 *Interiors*, 236, 36–51. <https://doi.org/10.1016/j.pepi.2014.08.004>
- 379 Dumoulin, C., Tobie, G., Verhoeven, O., Rosenblatt, P., & Rambaux, N. (2017). Tidal  
380 constraints on the interior of Venus. *Journal of Geophysical Research: Planets*, 122(6),  
381 1338–1352. <https://doi.org/10.1002/2016JE005249>
- 382 Elkins-Tanton, L. T. (2012). Magma Oceans in the Inner Solar System. *Annual Review of Earth*  
383 *and Planetary Sciences*, 40(1), 113–139. [https://doi.org/10.1146/annurev-earth-042711-](https://doi.org/10.1146/annurev-earth-042711-105503)  
384 105503
- 385 Gillmann, C., & Tackley, P. (2014). Atmosphere/mantle coupling and feedbacks on Venus.  
386 *Journal of Geophysical Research: Planets*, 119(6), 1189–1217.  
387 <https://doi.org/10.1002/2013JE004505>
- 388 Gillmann, C., Chassefière, E., & Lognonné, P. (2009). A consistent picture of early  
389 hydrodynamic escape of Venus atmosphere explaining present Ne and Ar isotopic ratios  
390 and low oxygen atmospheric content. *Earth and Planetary Science Letters*, 286(3–4), 503–  
391 513. <https://doi.org/10.1016/j.epsl.2009.07.016>
- 392 Gillmann, C., Golabek, G. J., & Tackley, P. J. (2016). Effect of a single large impact on the  
393 coupled atmosphere-interior evolution of Venus. *Icarus*, 268, 295–312.  
394 <https://doi.org/10.1016/j.icarus.2015.12.024>
- 395 Hamano, K., Abe, Y., & Genda, H. (2013). Emergence of two types of terrestrial planet on  
396 solidification of magma ocean. *Nature*, 497(7451), 607–10.  
397 <https://doi.org/10.1038/nature12163>
- 398 Hirose, K., Labrosse, S., & Hernlund, J. (2013). Composition and State of the Core. *Annual*  
399 *Review of Earth and Planetary Sciences*, 41(1), 657–691. [https://doi.org/10.1146/annurev-](https://doi.org/10.1146/annurev-earth-050212-124007)  
400 earth-050212-124007
- 401 Holmström, E., Stixrude, L., Scipioni, R., & Foster, A. S. (2018). Electronic conductivity of  
402 solid and liquid (Mg, Fe)O computed from first principles. *Earth and Planetary Science*  
403 *Letters*, 490, 11–19. <https://doi.org/10.1016/j.epsl.2018.03.009>
- 404 Ikoma, M., Elkins-Tanton, L., Hamano, K., & Suckale, J. (2018). Water Partitioning in Planetary  
405 Embryos and Protoplanets with Magma Oceans. *Space Science Reviews*, 214(4), 1–28.  
406 <https://doi.org/10.1007/s11214-018-0508-3>
- 407 Jacobson, S. A., Rubie, D. C., Hernlund, J., Morbidelli, A., & Nakajima, M. (2017). Formation,  
408 stratification, and mixing of the cores of Earth and Venus. *Earth and Planetary Science*  
409 *Letters*, 474, 375–386. <https://doi.org/10.1016/j.epsl.2017.06.023>
- 410 Kaula, W. (1999). Constraints on Venus Evolution from Radiogenic Argon. *Icarus*, 139(1), 32–  
411 39. <https://doi.org/10.1006/icar.1999.6082>

- 412 Konôpková, Z., McWilliams, R. S., Gómez-Pérez, N., & Goncharov, A. F. (2016). Direct  
413 measurement of thermal conductivity in solid iron at planetary core conditions. *Nature*,  
414 534(7605), 99–101. <https://doi.org/10.1038/nature18009>
- 415 Konopliv, A. S., & Yoder, C. F. (1996). Venusian k2 tidal Love number from Magellan and  
416 PVO tracking data. *Geophysical Research Letters*, 23(14), 1857–1860.  
417 <https://doi.org/10.1029/96gl01589>
- 418 Korenaga, J. (2008). Urey ratio and the structure and evolution of Earth's mantle. *Reviews of*  
419 *Geophysics*, 46(2), RG2007. <https://doi.org/10.1029/2007RG000241>
- 420 Labrosse, S. (2015). Thermal evolution of the core with a high thermal conductivity. *Physics of*  
421 *the Earth and Planetary Interiors*, 247, 36–55. <https://doi.org/10.1016/j.pepi.2015.02.002>
- 422 Labrosse, S., Hernlund, J. W., & Coltice, N. (2007). A crystallizing dense magma ocean at the  
423 base of the Earth's mantle. *Nature*, 450(7171), 866–9. Retrieved from  
424 <http://dx.doi.org/10.1038/nature06355>
- 425 Landeau, M., Aubert, J., & Olson, P. (2017). The signature of inner-core nucleation on the  
426 geodynamo. *Earth and Planetary Science Letters*, 465, 193–204.  
427 <https://doi.org/10.1016/j.epsl.2017.02.004>
- 428 Laneuville, M., Hernlund, J., Labrosse, S., & Guttenberg, N. (2017). Crystallization of a  
429 compositionally stratified basal magma ocean. *Physics of the Earth and Planetary Interiors*.  
430 <https://doi.org/10.1016/j.pepi.2017.07.007>
- 431 Lay, T., Hernlund, J., & Buffett, B. A. (2008). Core–mantle boundary heat flow. *Nature*  
432 *Geoscience*, 1(1), 25–32. <https://doi.org/10.1038/ngeo.2007.44>
- 433 Li, M., McNamara, A. K., Garnero, E. J., & Yu, S. (2017). Compositionally-distinct ultra-low  
434 velocity zones on Earth's core-mantle boundary. *Nature Communications*, 8(1).  
435 <https://doi.org/10.1038/s41467-017-00219-x>
- 436 Mosenfelder, J. L., Asimow, P. D., & Ahrens, T. J. (2007). Thermodynamic properties of  
437 Mg<sub>2</sub>SiO<sub>4</sub> liquid at ultra-high pressures from shock measurements to 200 GPa on forsterite  
438 and wadsleyite. *Journal of Geophysical Research: Solid Earth*, 112(6).  
439 <https://doi.org/10.1029/2006JB004364>
- 440 Nakagawa, T., & Tackley, P. J. (2010). Influence of initial CMB temperature and other  
441 parameters on the thermal evolution of Earth's core resulting from thermochemical  
442 spherical mantle convection. *Geochemistry Geophysics Geosystems*, 11(6).  
443 <https://doi.org/10.1029/2010GC003031>
- 444 Nakagawa, T., & Tackley, P. J. (2015). Influence of plate tectonic mode on the coupled  
445 thermochemical evolution of Earth's mantle and core. *Geochemistry Geophysics*  
446 *Geosystems*, 16, 3400–3413. <https://doi.org/10.1002/2015GC005996>
- 447 Nakajima, M., & Stevenson, D. J. (2015). Melting and mixing states of the Earth's mantle after

- 448 the Moon-forming impact. *Earth and Planetary Science Letters*, 427, 286–295.  
449 <https://doi.org/10.1016/j.epsl.2015.06.023>
- 450 Namiki, N., & Solomon, S. C. (1998). Volcanic degassing of argon and helium and the history of  
451 crustal production on Venus. *Journal of Geophysical Research*, 103(E2), 3655.  
452 <https://doi.org/10.1029/97JE03032>
- 453 Nimmo, F. (2015). Thermal and Compositional Evolution of the Core. In *Treatise on*  
454 *Geochemistry: Second Edition* (Vol. 9, pp. 217–241). Elsevier B.V.  
455 <https://doi.org/10.1016/B978-044452748-6.00147-4>
- 456 O'Rourke, J. G., & Korenaga, J. (2015). Thermal evolution of Venus with argon degassing.  
457 *Icarus*, 260, 128–140. <https://doi.org/10.1016/j.icarus.2015.07.009>
- 458 O'Rourke, J. G., & Stevenson, D. J. (2016). Powering Earth's dynamo with magnesium  
459 precipitation from the core. *Nature*, 529(7586), 387–389.  
460 <https://doi.org/10.1038/nature16495>
- 461 O'Rourke, J. G., Korenaga, J., & Stevenson, D. J. (2017). Thermal evolution of Earth with  
462 magnesium precipitation in the core. *Earth and Planetary Science Letters*, 458, 263–272.  
463 <https://doi.org/10.1016/j.epsl.2016.10.057>
- 464 O'Rourke, J. G., Gillmann, C., & Tackley, P. (2018). Prospects for an ancient dynamo and  
465 modern crustal remanent magnetism on Venus. *Earth and Planetary Science Letters*, 502,  
466 46–56. <https://doi.org/10.1016/j.epsl.2018.08.055>
- 467 O'Rourke, J. G., Buz, J., Fu, R. R., & Lillis, R. J. (2019). Detectability of Remanent Magnetism  
468 in the Crust of Venus. *Geophysical Research Letters*, 46, 2019GL082725.  
469 <https://doi.org/10.1029/2019GL082725>
- 470 Ohta, K., Yagi, T., Taketoshi, N., Hirose, K., Komabayashi, T., Baba, T., et al. (2012). Lattice  
471 thermal conductivity of MgSiO<sub>3</sub> perovskite and post-perovskite at the core-mantle  
472 boundary. *Earth and Planetary Science Letters*, 349–350, 109–115.  
473 <https://doi.org/10.1016/j.epsl.2012.06.043>
- 474 Ohta, K., Kuwayama, Y., Hirose, K., Shimizu, K., & Ohishi, Y. (2016). Experimental  
475 determination of the electrical resistivity of iron at Earth's core conditions. *Nature*,  
476 534(7605), 95–98. <https://doi.org/10.1038/nature17957>
- 477 Phillips, J. L., & Russell, C. T. (1987). Upper limit on the intrinsic magnetic field of Venus.  
478 *Journal of Geophysical Research*, 92(A3), 2253. <https://doi.org/10.1029/JA092iA03p02253>
- 479 Pozzo, M., Davies, C., Gubbins, D., & Alfè, D. (2019). FeO Content of Earth's Liquid Core.  
480 *Physical Review X*, 9(4), 041018. <https://doi.org/10.1103/PhysRevX.9.041018>
- 481 Scipioni, R., Stixrude, L., & Desjarlais, M. P. (2017). Electrical conductivity of SiO<sub>2</sub> at extreme  
482 conditions and planetary dynamos. *Proceedings of the National Academy of Sciences of the*  
483 *United States of America*, 114(34), 9009–9013. <https://doi.org/10.1073/pnas.1704762114>

- 484 Smrekar, S. E., Davaille, A., & Sotin, C. (2018). Venus Interior Structure and Dynamics. *Space*  
485 *Science Reviews*, 214(5), 88. <https://doi.org/10.1007/s11214-018-0518-1>
- 486 Soubiran, F., & Militzer, B. (2018). Electrical conductivity and magnetic dynamos in magma  
487 oceans of Super-Earths. *Nature Communications*, 9(1). [https://doi.org/10.1038/s41467-018-](https://doi.org/10.1038/s41467-018-06432-6)  
488 06432-6
- 489 Stevenson, D. J. (2003). Planetary magnetic fields. *Earth and Planetary Science Letters*, 208(1–  
490 2), 1–11. [https://doi.org/10.1016/S0012-821X\(02\)01126-3](https://doi.org/10.1016/S0012-821X(02)01126-3)
- 491 Stixrude, L., & Karki, B. (2005). Structure and Freezing of MgSiO<sub>3</sub> Liquid in Earth's Lower  
492 Mantle. *Science*, 310(5746), 297–299. <https://doi.org/10.1126/science.1116952>
- 493 Tang, F., Taylor, R. J. M., Einsle, J. F., Borlina, C. S., Fu, R. R., Weiss, B. P., et al. (2019).  
494 Secondary magnetite in ancient zircon precludes analysis of a Hadean geodynamo.  
495 *Proceedings of the National Academy of Sciences*, 116(2), 407–412.  
496 <https://doi.org/10.1073/pnas.1811074116>
- 497 Ulvrová, M., Labrosse, S., Coltice, N., Råback, P., & Tackley, P. J. (2012). Numerical modelling  
498 of convection interacting with a melting and solidification front: Application to the thermal  
499 evolution of the basal magma ocean. *Physics of the Earth and Planetary Interiors*, 206–207,  
500 51–66. <https://doi.org/10.1016/j.pepi.2012.06.008>
- 501 Way, M. J., Del Genio, A. D., Kiang, N. Y., Sohl, L. E., Grinspoon, D. H., Aleinov, I., et al.  
502 (2016). Was Venus the first habitable world of our solar system? *Geophysical Research*  
503 *Letters*, 43(16), 8376–8383. <https://doi.org/10.1002/2016GL069790>
- 504 Weiss, B. P., Maloof, A. C., Tailby, N., Ramezani, J., Fu, R. R., Hanus, V., et al. (2015).  
505 Pervasive remagnetization of detrital zircon host rocks in the Jack Hills, Western Australia  
506 and implications for records of the early geodynamo. *Earth and Planetary Science Letters*,  
507 430, 115–128. <https://doi.org/10.1016/j.epsl.2015.07.067>
- 508 Weller, M. B., & Kiefer, W. S. (2019). The Physics of Changing Tectonic Regimes: Implications  
509 for the Temporal Evolution of Mantle Convection and the Thermal History of Venus.  
510 *Journal of Geophysical Research: Planets*, 2019JE005960.  
511 <https://doi.org/10.1029/2019JE005960>
- 512 Xie, S., & Tackley, P. J. (2004). Evolution of helium and argon isotopes in a convecting mantle.  
513 *Physics of the Earth and Planetary Interiors*, 146(3–4), 417–439.  
514 <https://doi.org/10.1016/j.pepi.2004.04.003>
- 515 Yoder, C. F. (1995). Venus' Free Obliquity. *Icarus*, 117(2), 250–286.  
516 <https://doi.org/10.1006/icar.1995.1156>
- 517 Zhang, Z., Dorfman, S. M., Labidi, J., Zhang, S., Li, M., Manga, M., et al. (2016). Primordial  
518 metallic melt in the deep mantle. *Geophysical Research Letters*, 43(8), 3693–3699.  
519 <https://doi.org/10.1002/2016GL068560>

520 Ziegler, L. B., & Stegman, D. R. (2013). Implications of a long-lived basal magma ocean in  
521 generating Earth's ancient magnetic field. *Geochemistry, Geophysics, Geosystems*, *14*(11),  
522 4735–4742. <https://doi.org/10.1002/2013GC005001>

523